International Journal of Applied Power Engineering (IJAPE)
Vol. 15, No. 2, June 2026, pp. 744~759
ISSN: 2252-8792, DOI: 10.11591/ijape.v15.i2.pp744-759

Stochastic planning for feeding a green hydrogen plant into an isolated network

Michael Salcedo, Mario A. Rios
Department of Electrical and Electronics Engineering, School of Engineering, University de los Andes, Bogotá, Colombia

Article Info

Article history:

Received Aug 8, 2025
Revised Jan 27, 2026
Accepted Mar 12, 2026

Keywords:

Autoregressive moving average
Dynamic optimization
Green hydrogen
Sequential Monte Carlo
Wind power variability

ABSTRACT

In recent years, an electrochemical process called electrolysis has gained prominence. This process uses water and electricity as its main sources, significantly reducing the carbon footprint of hydrogen production. Additionally, colors have been assigned to represent the source of hydrogen production in a simple way. For example, green refers to hydrogen produced by electrolysis using electricity generated from non-conventional renewable energy sources (NCRES). For plants not connected to the national grid, the connection of a green hydrogen plant requires that NCRES be connected to an isolated electrical grid. In these cases, the power supply will depend on the variability of the source. This paper presents the methodology to plan and size the main components of the wind power plant and the battery energy storage system (BESS) to ensure that the electrolyzer constraints can be met during the studied period. Furthermore, it introduces a novel methodology that uses the autoregressive moving average (ARMA) model to generate a sequential Monte Carlo simulation along with dynamic optimization. This approach allows for the sizing of the wind power plant and BESS, considering the stochastic behavior of the wind.

Corresponding Author:

Mario A. Rios
Department of Electrical and Electronics Engineering, School of Engineering, Universidad de los Andes
Cra 1 Este N° 19A – 40, Edificio Mario Laserna ML-736, Bogotá, Colombia
Email: mrios@uniandes.edu.co

1. INTRODUCTION

Due to the recent interest in reducing global warming, one of the main causes of CO_2 emissions is primarily from the combustion of coal and hydrocarbon derivatives. Consequently, governments and the industrial sector have been developing measures to reduce the carbon footprint of these processes. A key element in this effort is hydrogen, which is a crucial component in various sectors such as petrochemicals, the food industry, coal mining, and iron production. Examples of raw materials that involve hydrogen include ammonia, ethanol, and urea. However, hydrogen production has traditionally relied on petrochemical processes that use hydrocarbons or coal as sources. Fortunately, in recent years, an electrochemical process called electrolysis has gained prominence. This process uses water and electricity as its main components. Additionally, colors have been assigned to represent the source of hydrogen production: green refers to hydrogen produced by electrolysis using electricity generated from non-conventional renewable energy sources (NCRES) [1].

The primary strategy for supplying electrical power to a green hydrogen plant is to use the national grid. Normally, a contract with a generation company ensures the energy service from NCRES during the specified period. Consequently, the electrolyzer arrays are subjected to the same electrical quality parameters (continuity, reliability) as a typical industrial plant [2], [3]. However, in remote areas such as coal mines or gas production plants, where there is no connection to the national grid, the green hydrogen plant must be connected to an isolated grid powered by NCRES.

Several research works have been carried out to present strategies to allocate, schedule or size NCRES, battery energy storage system (BESS) and hydrogen production plants; for instance, in [4] it is formulated a mixed-integer quadratically-constrained programming (MIQCP) optimization problem to minimize the total present value cost of the power system, where it is aborded the hydrogen production constraints and the location of photovoltaic systems in a weak grid, by the other hand [5] gives an strategy to locate the BESS in a grid under high wind power penetration, using heuristic optimization technique in order to minimize energy losses in the grid. On the other hand, in [6], it presents a multiperiod power flow to optimize the dispatch of the sources including photovoltaic (PV) and BESS in distribution grid where also it is used a mixed-integer nonlinear programming (MINLP) optimization with autoregressive parameters (ARMA) in order to predict the load, Morais *et al*. [7] presents a linearized model using mixed-integer linear programming (MILP) to reduce the marginal cost in non-isolated grid compounds of PV system, fuel cell and an wind power plant, and Sherature *et al*. [8] propose an strategy to schedule the electricity excess in an isolated area using a hybrid optimization model. Other researches have focused on providing methods of rating the main components, in [3], it presents a MILP model in order to size the optimal size of a electrolzyer array based on a due wind plant characteristics, by the other hand [9], [10] proposes a similar MILP model, but in this case to size the BESS and wind plant considering an extra diesel generator to feed an residential load. Pan *et al*. [11] approaches the PV, wind power plant, and storage capacity proportion to produce hydrogen, in this is incorporated the time series. Finally, Dawoud *et al*. [12] presents a state of art of the different optimization methods to size the isolated grid components, but based on different function objectives, such as for example power supply probability, investment cost, and the deterministic optimization methods, such as hybrid SPV, PSO, and LOLP.

Thus, this paper presents a strategy to size the major components in insolated grid due to the required yearly average hydrogen production. These major components are the wind power plant and BESS. Given that Eolic energy depends on the wind speed, and it is known that it presents stochastic behavior, because of that, it is necessary to establish the hydrogen production constraints in terms of electrical power supply. Then, through stochastic optimization tools it can obtain the rated parameter of the wind farm and battery. In section 2, the general concepts of green hydrogen production, and electrical requirements are presented, the BESS model to be implemented, and the first approach to the stochastic optimization bases is presented in section 3, the methodology is explained where the two cases of the isolated grid to feed an electrolyzer array are detailed, where the first one only considers a wind power plant and a BESS, and the other one an additional thermal generator, defining the constraints and objective functions to be minimized. Section 4 presents a case study. Section 5 presents the results of two test cases, and finally section 6 presents the conclusions of this paper.

2. THEORETICAL BASES

2.1. Green hydrogen definition

Nowadays, hydrogen production processes vary depending on the application and are used in various chemical processes, primarily in the petroleum and food industries. Due to the necessity of an energy transition, there is a global consensus on reducing CO_2 emissions into the atmosphere. Consequently, energy sources for producing different products or developing processes have increasingly focused on sustainability, leading to a rise in plants based on NCRES. Furthermore, an electrochemical process called electrolysis, which produces hydrogen by applying direct current to water, separates the water molecules into hydrogen and oxygen. This process has enabled the development of various technologies over the last twenty years, as it relies on electricity rather than directly on fuel combustibles [1], [13], [14]. Thus, a color spectrum has been defined to easily understand hydrogen production based on the source and material used, ultimately summarizing the CO_2 emissions into the atmosphere, as shown in Table 1.

Table 1. Color classification of hydrogen production [13]

Color	Process	Source	CO_2 emissions
Black	Gasification	Coal	Hight
Gray	Steam reforming	Natural gas	High
Blue	Steam reforming with carbon capture	Natural gas	Low
Cian	Pyrolysis	Natural gas	Non direct CO_2 emissions
Green	Electrolysis	Water/electricity from renewable energy plants	Non direct CO_2 emissions
Rose	Electrolysis	Water/electricity from nuclear energy plants	Non direct CO_2 emissions
Yellow	Electrolysis	Water/electricity from solar energy plants	Non direct CO_2 emissions

2.2. Electrolysis process

Today, various technologies exist that utilize electrochemical processes to separate water molecules into hydrogen (H2) and oxygen (O). These technologies are [1], [14]: alkaline (ALK), proton exchange membrane (PEM), solid oxide electrolyzer (SOE), and anion exchange membrane (AEM). ALK and PEM technologies are the most developed industrially, making them the most widely used. This paper focuses on PEM technology due to its advantages, such as the non-replacement of parts during its lifetime and its quick activation time.

2.3. PEM electrolyzer

This type of electrolyzer uses a proton exchange membrane as the separator between the anode and cathode. When a direct current is applied, water is separated into H2 and O, with hydrogen protons passing through the membrane to form hydrogen gas on the cathode side [1], [15]. Figure 1 shows a schematic of the PEM process. The advantages of this technology include its efficiency at low temperatures and its compact size compared to other types of electrolyzers. However, some of its components, such as platinum, are precious metals, which increases the cost [16].

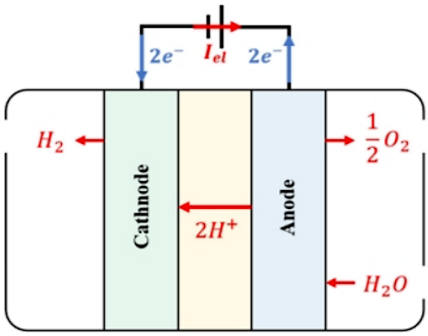

Figure 1. PEM process schematic [1]

2.4. Electrical power supply requirements

The objective of the power supply is to maximize efficiency during the electrolysis process, improve the purity of hydrogen, and extend the lifetime of the electrolyzer while achieving the polarization curve [4], [13], [17], [18]. Figure 2 shows the schematic diagram of the electrolysis supply of power [19]. In addition, the following constraints must be met at the electrolyzer point of power supply [4], [17], [20]. The current density is related to voltage input and temperature. For a determined temperature it is a current density point that produces better efficiency, and hydrogen production relates positivity with current density.

2.5. BESS model

Figure 3 presents a straightforward model that illustrates the main parameters, thereby explaining the behavior of the BESS as follows [9], [21], [22]:

i) Only two stages are considered: charge and discharge. The standby mode is neglected for this analysis.
ii) P_B represents the state of charge, operating within the range of minimum B_{min} and maximum B_{max} values, multiplied by the BESS rating P_{RB}.
iii) P_{CB} denotes the energy absorbed by the grid during discharge, accounting for self-load discharge (SLD) and charge process losses, which depend on the load charge efficiency e_{CB}.
iv) P_{DB} signifies the energy delivered to the grid during charge, considering SLD and discharge process losses, which depend on the load discharge efficiency e_{DB}.
v) Additionally, the curve slope must remain within the limits specified by the manufacturer, denoted by τ_B. Although this factor varies between the charge and discharge processes, this paper assumes symmetry for the analysis.

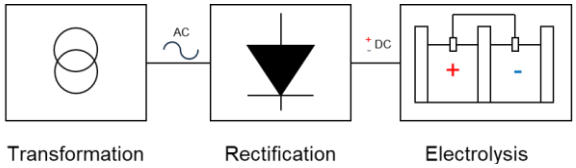

Figure 2. Simple schematic of electrolysis power supply [19]

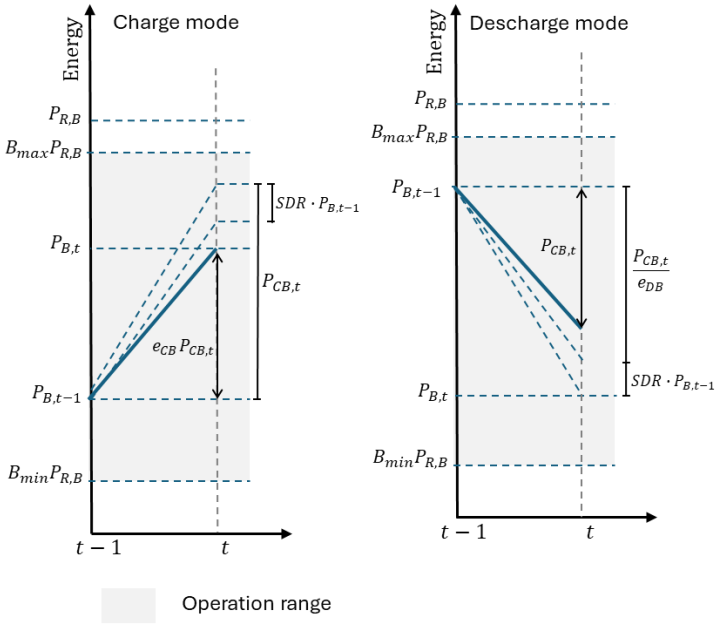

Figure 3. BESS behavior

2.6. Stochastic optimization

The problem to solve in this paper is to size the BESS and wind power plant, but the main energy resource is the wind. Furthermore, as previously mentioned, charge and discharge cycles limits depend on the rated values of the BESS, which is why it is also necessary to take into consideration the time. In consequence, a general optimization problem that considers stochastic aspects is the minimization of the objective function $F(x)$, as (1) [23].

$$\min \{F(x): G_t(x) \leq 0;\ \forall\, t = 1, \dots, T\} \tag{1}$$

Where: $G_i(x)$ is the set of restrictions at t, x is the vector of the variables to optimize, and t is the restriction. Due to these restrictions, do not consider stochasticity, another vector ξ is included, which is the vector of the random parameter ξ_t that follows a probability distribution. Thus, the optimization problem becomes (2).

$$\min \{F(x): G_t(x, \xi) \leq 0;\ \forall\, t = 1, \dots, T\} \tag{2}$$

The solution to this problem also yields a stochastic result. There are two ways to address this: first, through multistage stochastic optimization, and second, through dynamic optimization. Since our process involves charging and discharging batteries, dynamic optimization provides an accurate solution. Figure 4 illustrates the dynamic process.

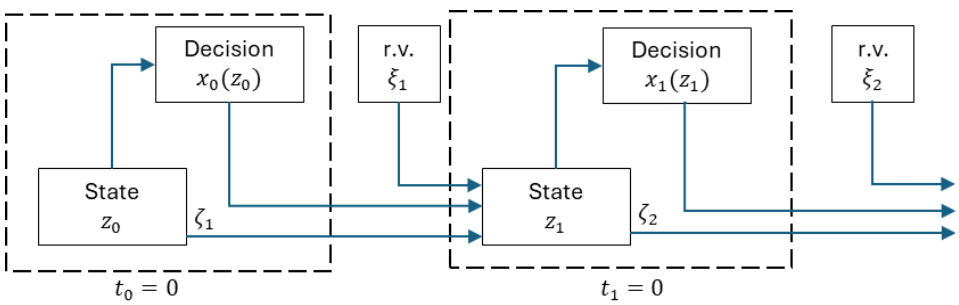

Figure 4. Dynamic optimization process [23]

Per each time t is defined as a state of the system ζ_t, and the state for each will depend on the past behavior and results [23].

$$\zeta_{t+1} = (x_0, \xi_1, x_1, \dots \xi_t) \tag{3}$$

Thus, this problem can be solved in state-space with the (4) [23].

$$\min \left\{ F(x) \coloneqq \mathcal{R}[(Q_1(\zeta_1),\ Q_2(\zeta_2), \dots, Q_T(\zeta_T))] \Big|_{\zeta_{t+1} = k_{t+1}(\zeta_t, x_t, \xi_{t+1}), t = 0, \dots, T-1}^{\zeta_0 = z_0,} \right\} \tag{4}$$

That means $F(x)$ is the objective function, Q_t is the set of restrictions for each time state, considering that each state depends on the previous state, and thus, the optimization problem complexity increases according to the time T to be studied.

2.7. ARMA model

Based on the previously defined optimization framework, it is necessary to incorporate a model capable of generating a wind speed time series. This is particularly important because available wind data is typically limited to short measurement periods. Moreover, the inclusion of a BESS, whose behavior depends on its previous state, requires a time-dependent modeling approach. To address these challenges, the ARMA model is employed to generate the required wind speed time series. The general form of the ARMA model is expressed as (5) [24].

$$x_t = \alpha_1 x_{t-1} + \cdots \alpha_p x_{t-p} + y_t + \beta_1 y + \cdots + \beta_q y \tag{5}$$

Where, t is the time, y is normal white; noise with normal distribution, mean 0, and variance σ_α. x_t is the value of the series at time t, α is the autoregressive parameter, β is the average sliding parameter, p is the autoregressive order, and q is the average sliding order. Thus, for the problem studied in this paper, the expected wind speed is given by (6) [2].

$$v_t = \mu + \sigma x_t \tag{6}$$

Where: v_t is expected wind speed for time t, μ is average wind speed of measurement data, and σ is standard deviation of measurement input data. The algorithms and analytical methods used to derive the ARMA model parameters are beyond the scope of this paper and are thoroughly discussed in [24]. For the purposes of this study, the econometrics module available in the commercial software MATLAB is employed to perform the necessary time series analysis.

3. METHODOLOGY

The proposed methodology is based in two scenarios (Figures 5(a) and 5(b)). In the first scenario, the system is designed to supply a green hydrogen plant with predefined hydrogen production requirements. As a result, the nominal power rating of the electrolyzer is treated as a fixed input, alongside the plant's operational loads, which include pumps, compressors, lighting, and other auxiliary systems shown in Figure 5(a).

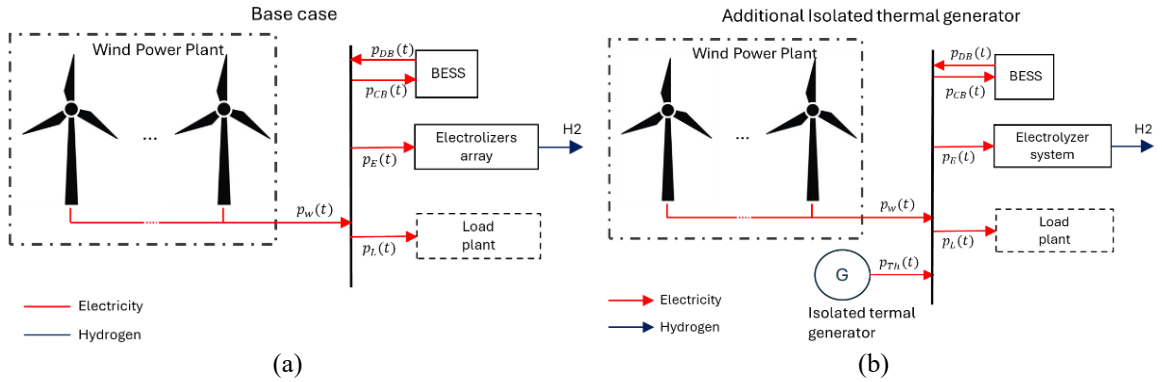

Figure 5. Study cases for green hydrogen plants connected to isolated grid: (a) fixed-demand system configuration and (b) constrained renewable system configuration

A wind power plant and a BESS provide the energy, both of which are expected to ensure continuous power delivery. In this configuration, the wind power plant injects energy into the grid, while the BESS either supplies or absorbs power depending on its operational mode. The system is assumed to include control mechanisms capable of managing power deficits or surpluses relative to the combined demand of the plant and the electrolyzer.

In the second scenario, the availability of renewable energy sources constrains the green hydrogen production. To address this, a thermal generator operating in isolated mode is introduced to supplement the energy supply during periods of insufficient wind generation. Figure 5(b) illustrates the second scenario.

3.1. Case 1

In case 1, as mentioned, hydrogen production is previously done by an electrolyzer array, which is assumed as an input given by the necessities of the process. In this case, the function to be minimized will be the levelized cost of hydrogen (LCOH), which is defined as (7) [3].

$$LCOH = \frac{CPF}{\sum_{t=1}^{N} m_{H2,t}} \tag{7}$$

Where $m_{H2,t}$ is the produced hydrogen, and CPF is the present cost of the investment (wind power plant, BESS, and electrolyzer array). Thus, CPF is calculated as (8) [3].

$$CPF = CAPEX + OPEX \tag{8}$$

Assuming that the OPEX is proportional to the CAPEX, the value of the CPF can then be determined, assuming installation values depending on the system unitary cost π, therefore, it can be possible to calculate the CPF with (9) [3].

$$CPF = \pi_w P_{R,w} + \pi_B P_{R,B} + \pi_E P_E \tag{9}$$

Where, π_w is the unit present cost of the wind power plant, π_B is the unit present cost of the BESS, π_E is the unit present cost of the BESS, $P_{R,w}$ is the rated power of the wind power plant, $P_{R,B}$ is the rated power of the BESS, and P_E is the rated power of the electrolyzer array.

3.1.1. Objective function case 1

Since the rated power of the electrolyzer is treated as a fixed input, hydrogen production remains nearly constant throughout the analysis period. As a result, the optimization problem is simplified to minimize the present investment cost associated with the wind power plant and the BESS. The objective function is therefore as (10) [3].

$$\min_x f(x) = \pi_w P_{R,w} + \pi_B P_{R,B} \tag{10}$$

3.1.2. Constraints case 1

This optimization problem is subject to several constraints, including power balance, operational limitations of the BESS, and performance requirements of the electrolyzer. These constraints must be satisfied at each time step t throughout the simulation horizon. Thus, the injected and consumed power must be equal; therefore, the (11) applies [3].

$$P_{w,t} + P_{DB,t} = P_{CB,t} + P_{E,t} + P_{L,t} + P_{dump,t} \tag{11}$$

Where, $P_{w,t}$ is the injected wind power, $P_{DB,t}$ is the BESS discharged energy, $P_{CB,t}$ is the BESS charged energy, $P_{E,t}$ is the electrolyzer's consumed power, $P_{L,t}$ is the load power, P_{dump} is the dump power, and t is the time. But, considering that wind power follows a similar distribution of only one turbine, the following relation is defined as (12).

$$P_{W,t} = \xi_t P_{R,w} \tag{12}$$

Where, $P_{R,W}$ is the rated power of the wind power plant, and ξ_t is the unit factor of the wind power generation. Thus, replacing in previous equation, the power balance equality is as (13).

$$\xi_t P_{R,w} + P_{DB,t} = P_{CB,t} + P_{E,t} + P_{L,t} + P_{dump};\ \xi_t \epsilon[0,1] \quad (13)$$

The BESS constraints pertain to the state of charge, which depends on the previous stage as well as the discharge or charge, as (14) [3].

$$P_{B,t} = (1 - SDR)P_{B,t-1} + e_{cb}P_{CB,t} - \frac{P_{DB,t}}{e_{db}} \quad (14)$$

Where $P_{B,t}$ is the BESS stage of charge, SDR is the BESS self-discharge ratio, e_{cb} is the BESS charging efficiency, and e_{cd} is the BESS discharging efficiency. BESS is only charged or uncharged at any time:

$$\left.\begin{matrix} P_{CB,t} = \alpha_t P_{B,max} \\ P_{DB,t} = (1 - \alpha_t)\, P_{B,max} \end{matrix}\right\};\ \alpha_t \epsilon[0,1] \quad (15)$$

Thus, α_t can be 0 or 1, which conditionates that if $P_{CB,t}$ is positive, $P_{DB,t}$ will be 0, but in the opposite case, $P_{DB,t}$ is positive, $P_{CB,t}$ will be 0 [3], [25].

As previously mentioned, the rate at which the BESS is charged or discharged will be limited by the following factors [3].

$$\frac{1}{\tau_B} P_{R,B} \leq P_{B,t} - P_{B,t-1} \leq \frac{1}{\tau_B} P_{R,B} \quad (16)$$

Where τ_B is the BESS charge/discharge ratio, and BESS state of charge should be under the operation limits:

$$b^B_{min} P_{R,B} \leq P_{B,t} \leq b^B_{max} P_{R,B} \quad (17)$$

where, b^B_{min}: is the BESS minimum limit of charge; and b^B_{max}: is the BESS maximum limit of charge.

In the case of the initial state of charge, this value is not arbitrarily assigned but is instead treated as a decision variable within the optimization process. The lower bound is not enforced, allowing the BESS to begin operation in a fully discharged state [3].

$$P_{B,0} \leq b^B_{max} P_{R,B} \quad (18)$$

The final constraint in the optimization problem pertains to the power requirements of the electrolyzer. To ensure proper operation, the supplied power must remain within the specified operational limits at each time step.

$$b^E_{min} P_{R,E} \leq P_{E,t} \leq b^E_{max} P_{R,E} \quad (19)$$

3.2. Case 2

In case 2, an additional thermal generator is incorporated into the system. As a result, the power balance equation is modified to include the energy injected by the thermal plant, which supplements the wind and BESS contributions during periods of insufficient renewable generation.

$$\xi_t P_{W,t} + P_{DB,t} + P_{Th,t} = P_{CB,t} + P_{E,t} + P_{L,t} + P_{dump} \quad (20)$$

Where $P_{Th,t}$ is the thermal plant's injected power, and $P_{Th,t}$ operates under (21).

$$P^{min}_{Th} \leq P_{Th,t} \leq P^{max}_{Th} \quad (21)$$

Accordingly, the objective function is expanded to include the cost of thermal energy generation over the analysis period.

$$\min_x f(x) = \pi_w P_{R,w} + \pi_B P_{R,B} + \pi_{TH} \sum_{t=1}^{N} P_{th,t} \quad (22)$$

Where π_{TH} is the unit price of consumed energy of the thermal generator.

3.3. Optimization process

Considering the constraints previously defined, the overall optimization framework is illustrated in Figure 6 [6]. This schematic outlines the process used to solve the optimization problem under the conditions specified for both case studies. For each period, the following general optimization process shall be performed.

$$\min \left\{ F(x) = c^T x \;\middle|\; \begin{matrix} Ax \leq b \\ A_{eq}x = b_{eq} \\ x \in [l_b, u_b] \wedge \in \mathcal{R} \\ \alpha_t \in [0,1] \wedge \mathbb{Z} \forall\ t = 1,2,\cdots,N \end{matrix} \right\} \tag{23}$$

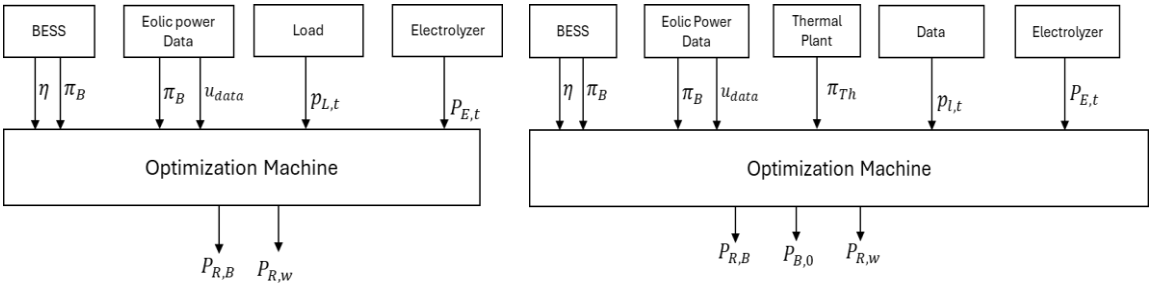

Figure 6. Optimization machine schematic for (a) case 1 and (b) case 2

3.3.1. Case 1

The optimization variable vector is divided into two stages. The first stage includes only the fixed variables to be optimized, which remain constant throughout the simulation horizon [4], [17].

$$x_{s1} = [P_{R,B} \quad P_{R,w} \quad P_{B,0}] \tag{24}$$

The second stage includes all time-dependent variables, which vary throughout the simulation horizon and are evaluated at each time step.

$$x_{s2,t} = [P_{CB,t} \quad P_{DB,t} \quad \alpha_t \quad P_{B,t} \quad P_{dump,t} \quad P_{E,t}] \tag{25}$$

Thus, the complete optimization variable vector is constructed by combining the fixed variables from the first stage with the time-dependent variables from the second stage, evaluated across the entire simulation horizon.

$$x = [x_{s1} \quad x_{s2,1} \quad \cdots \quad x_{s2,t} \quad \ldots \quad x_{s2,N}] \tag{26}$$

In this stage, the cost vector is defined based on the unit installation costs of the wind power plant and the BESS. These costs are treated as fixed parameters and are used to evaluate the total investment required for the system configuration.

$$c = [\pi_B \quad \pi_w \quad 0 \quad \ldots \quad 0] \tag{27}$$

In the case of the matrix, a similar approach is taken.

$$a_0 = \begin{bmatrix} 0 & 0 & 0 \\ 0 & 0 & 0 \\ -b^b_{max} & 0 & 0 \\ b_{min} & 0 & 0 \\ -\frac{1}{\tau_B} & 0 & -1 \\ -\frac{1}{\tau_B} & 0 & -1 \\ -1 & 0 & 1 \end{bmatrix}; a_1 = \begin{bmatrix} 1 & 0 & -P_{B,max} & 0 & 0 & 0 \\ 0 & 1 & P_{B,max} & 0 & 0 & 0 \\ 0 & 0 & 0 & 1 & 0 & 0 \\ 0 & 0 & 0 & -1 & 0 & 0 \\ 0 & 0 & 0 & 1 & 0 & 0 \\ 0 & 0 & 0 & -1 & 0 & 0 \\ 0 & 0 & 0 & 0 & 0 & 0 \end{bmatrix} \tag{28}$$

$$a_2 = \begin{bmatrix} 0 & 0 & 0 \\ 0 & 0 & 0 \\ -b_{max}^{b} & 0 & 0 \\ b_{min} & 0 & 0 \\ -\frac{1}{\tau_B} & 0 & 0 \\ -\frac{1}{\tau_B} & 0 & 0 \end{bmatrix}; a_3 = \begin{bmatrix} 0 & 0 & 0 & 0 & 0 & 0 \\ 0 & 0 & 0 & 0 & 0 & 0 \\ 0 & 0 & 0 & 0 & 0 & 0 \\ 0 & 0 & 0 & 0 & 0 & 0 \\ 0 & 0 & 0 & -1 & 0 & 0 \\ 0 & 0 & 0 & 1 & 0 & 0 \end{bmatrix} \quad (1)$$

Accordingly, matrix A is constructed based on the defined time window over which the optimization process is executed. This matrix incorporates the system constraints and variable relationships across all time steps within the simulation horizon.

$$A = \begin{matrix} t_0 & t_1 & t_2 & \cdots & \cdots & \cdots & t_N \end{matrix} \begin{bmatrix} a_0 & a_1 & \emptyset & \cdots & \cdots & \cdots & \emptyset \\ a_2 & a_3 & a_4 & \emptyset & \cdots & \cdots & \emptyset \\ a_2 & \emptyset & a_3 & a_4 & \emptyset & \cdots & \emptyset \\ \vdots & \vdots & \vdots & \vdots & \vdots & \vdots & \vdots \\ a_2 & \emptyset & \cdots & \cdots & \emptyset & a_3 & a_4 \end{bmatrix}; b = \begin{bmatrix} b_1 \\ b_2 \\ \vdots \\ b_2 \end{bmatrix} \begin{matrix} t_1 \\ t_2 \\ \vdots \\ t_N \end{matrix} \quad (30)$$

$$a_{eq0,1} = \begin{bmatrix} 0 & \xi_0 & 0 \\ 0 & 0 & -1 \end{bmatrix}; a_{eq1} = \begin{bmatrix} -1 & 1 & 0 & 0 & -1 & -1 \\ -e_{cb} & \frac{1}{e_{db}} & 0 & 1 & 0 & 0 \end{bmatrix} \quad (31)$$

$$a_{eq0,t} = \begin{bmatrix} 0 & 0 & 0 \\ 0 & \xi_t & 0 \end{bmatrix}; a_{eq2} = \begin{bmatrix} 0 & 0 & 0 & 0 & 0 & 0 \\ 0 & 0 & 0 & -1 & 0 & 0 \end{bmatrix} \quad (32)$$

$$A_{eq} = \begin{matrix} t_0 & t_1 & t_2 & & \cdots & \cdots & \cdots & t_N \end{matrix} \begin{bmatrix} a_{eq0,1} & a_{eq1} & \emptyset & \cdots & \cdots & \cdots & \emptyset \\ a_{eq0,2} & a_{eq2} & a_{eq1} & \emptyset & \cdots & \cdots & \emptyset \\ a_{eq0,3} & \emptyset & a_{eq2} & a_{ae1} & \emptyset & \cdots & \emptyset \\ \vdots & \vdots & \vdots & \vdots & \vdots & \vdots & \vdots \\ a_{eq0,N} & \emptyset & \cdots & \cdots & \emptyset & a_{eq2} & a_{eq3} \end{bmatrix}; b_{eq} = \begin{bmatrix} b_{eq1} \\ b_{eq1} \\ \vdots \\ b_{eq1} \end{bmatrix} \begin{matrix} t_1 \\ t_2 \\ \vdots \\ t_N \end{matrix} \quad (33)$$

3.3.2. Case 2

In this case, the vector of variables to be optimized in the first stage remains unchanged from the previous scenario.

$$x_{s1} = [P_{R,B} \quad P_{R,w} \quad P_{B,0}] \quad (34)$$

The second stage incorporates the power generated by the thermal plant at each step. This additional energy source is considered alongside the wind and BESS contributions to ensure that the system meets the total power demand throughout the simulation horizon.

$$x_{s2,t} = [P_{CB,t} \quad P_{DB,t} \quad \alpha_t \quad P_{B,t} \quad P_{dump,t} \quad P_{E,t} \quad P_{Th,t}] \quad (35)$$

The cost vector is divided into two distinct components. The first corresponds to the fixed installation costs of the wind power plant and the BESS, while the second accounts for the operational costs associated with thermal energy generation over the simulation period.

$$c_{s1} = [\pi_B \quad \pi_w \quad 0] \quad (36)$$

$$c_{s2} = [0 \quad 0 \quad 0 \quad 0 \quad 0 \quad 0 \quad \pi_{Th}] \quad (37)$$

Thus, the complete cost vector is constructed by combining the fixed installation costs of the wind power plant and BESS with the time-dependent operational costs of the thermal generator, evaluated across the entire simulation horizon.

$$c = [c_{s1} \quad c_{s2} \quad \cdots \quad c_{s2}] \quad (38)$$

For subarrays, the following conditions are incorporated.

$$a_0 = \begin{bmatrix} 0 & 0 & 0 \\ 0 & 0 & 0 \\ -b_{max}^{b} & 0 & 0 \\ b_{min} & 0 & 0 \\ -\frac{1}{\tau_B} & 0 & -1 \\ -\frac{1}{\tau_B} & 0 & -1 \\ -1 & 0 & 1 \\ 0 & -\sum_1^N \xi_t & 0 \end{bmatrix};\ a_1 = \begin{bmatrix} 1 & 0 & -P_{B,max} & 0 & 0 & 0 & 0 \\ 0 & 1 & P_{B,max} & 0 & 0 & 0 & 0 \\ 0 & 0 & 0 & 1 & 0 & 0 & 0 \\ 0 & 0 & 0 & -1 & 0 & 0 & 0 \\ 0 & 0 & 0 & 1 & 0 & 0 & 0 \\ 0 & 0 & 0 & -1 & 0 & 0 & 0 \\ 0 & 0 & 0 & 0 & 0 & 1 & 0 \end{bmatrix} \tag{39}$$

$$a_2 = \begin{bmatrix} 0 & 0 & 0 & 0 & 0 & 0 & 0 \\ 0 & 0 & 0 & 0 & 0 & 0 & 0 \\ 0 & 0 & 0 & 0 & 0 & 0 & 0 \\ 0 & 0 & 0 & 0 & 0 & 0 & 0 \\ 0 & 0 & 0 & 0 & 0 & 0 & 0 \\ 0 & 0 & 0 & 0 & 0 & 0 & 0 \\ 0 & 0 & 0 & 0 & 0 & 1 & 0 \end{bmatrix};\ a_3 = \begin{bmatrix} 0 & 0 \\ 0 & 0 \\ -b_{max}^{b} & 0 \\ b_{min} & 0 \\ -\frac{1}{\tau_B} & 0 \\ -\frac{1}{\tau_B} & 0 \end{bmatrix} \tag{40}$$

$$a_5 = \begin{bmatrix} 0 & 0 & 0 & 0 & 0 & 0 & 0 \\ 0 & 0 & 0 & 0 & 0 & 0 & 0 \\ 0 & 0 & 0 & 0 & 0 & 0 & 0 \\ 0 & 0 & 0 & 0 & 0 & 0 & 0 \\ 0 & 0 & 0 & 0 & -1 & 0 & 0 \\ 0 & 0 & 0 & 0 & 1 & 0 & 0 \end{bmatrix};\ a_5 = \begin{bmatrix} 1 & 0 & -P_{B,max} & 0 & 0 & 0 & 0 \\ 1 & 0 & P_{B,max} & 0 & 0 & 0 & 0 \\ 0 & 0 & 0 & 1 & 0 & 0 & 0 \\ 0 & 0 & 0 & -1 & 0 & 0 & 0 \\ 0 & 0 & 0 & 1 & 0 & 0 & 0 \\ 0 & 0 & 0 & -1 & 0 & 0 & 0 \end{bmatrix} \tag{41}$$

In this case, matrix A is constructed according to the defined time window over which the optimization process is executed. This matrix captures the temporal evolution of system constraints and variable interactions, enabling the formulation of a time-dependent optimization model.

$$A = \begin{matrix} t_0 & t_1 & t_2 & \cdots & \cdots & \cdots & t_N \end{matrix} \begin{bmatrix} a_0 & a_1 & a_2 & \cdots & \cdots & \cdots & a_2 \\ a_3 & a_4 & a_5 & \emptyset & \cdots & \cdots & \emptyset \\ a_3 & \emptyset & a_4 & a_5 & \emptyset & \cdots & \emptyset \\ \vdots & \vdots & \vdots & \vdots & \vdots & \vdots & \vdots \\ a_3 & \emptyset & \cdots & \cdots & \emptyset & a_4 & a_5 \end{bmatrix};\ b = \begin{bmatrix} b_1 \\ b_2 \\ \vdots \\ b_2 \end{bmatrix} \begin{matrix} t_1 \\ t_2 \\ \vdots \\ t_N \end{matrix} \tag{42}$$

$$a_{eq0,1} = \begin{bmatrix} 0 & 0 & -1 \\ 0 & \xi_0 & 0 \end{bmatrix};\ a_{eq1} = \begin{bmatrix} -1 & 1 & 0 & 0 & -1 & -1 & 1 \\ -e_{cb} & \frac{1}{e_{db}} & 0 & 1 & 0 & 0 & 0 \end{bmatrix} \tag{43}$$

$$a_{eq0,t} = \begin{bmatrix} 0 & 0 & 0 \\ 0 & \xi_t & 0 \end{bmatrix};\ a_{eq2} = \begin{bmatrix} 0 & 0 & 0 & 0 & 0 & 0 & 0 \\ 0 & 0 & 0 & -1 & 0 & 0 & 0 \end{bmatrix} \tag{44}$$

$$A_{eq} = \begin{matrix} t_0 & t_1 & t_2 & & \cdots & \cdots & \cdots & t_N \end{matrix} \begin{bmatrix} a_{eq0,1} & a_{eq1} & \emptyset & \cdots & \cdots & \cdots & \emptyset \\ a_{eq0,2} & a_{eq2} & a_{eq1} & \emptyset & \cdots & \cdots & \emptyset \\ a_{eq0,3} & \emptyset & a_{eq2} & a_{ae1} & \emptyset & \cdots & \emptyset \\ \vdots & \vdots & \vdots & \vdots & \vdots & \vdots & \vdots \\ a_{eq0,N} & \emptyset & \cdots & \cdots & \emptyset & a_{eq2} & a_{eq3} \end{bmatrix};\ b_{eq} = \begin{bmatrix} b_{eq1} \\ b_{eq2} \\ \vdots \\ b_{eq2} \end{bmatrix} \begin{matrix} t_1 \\ t_2 \\ \vdots \\ t_N \end{matrix} \tag{45}$$

3.3.3. Sequential Monte Carlo simulation

The construction of the matrices required for the general MILP optimization over the defined time window requires performing multiple realizations of the simulation. This repetition ensures a statistically robust sample, allowing for the generation of reliable stochastic results. The flow diagram illustrating this process is presented in Figure 7.

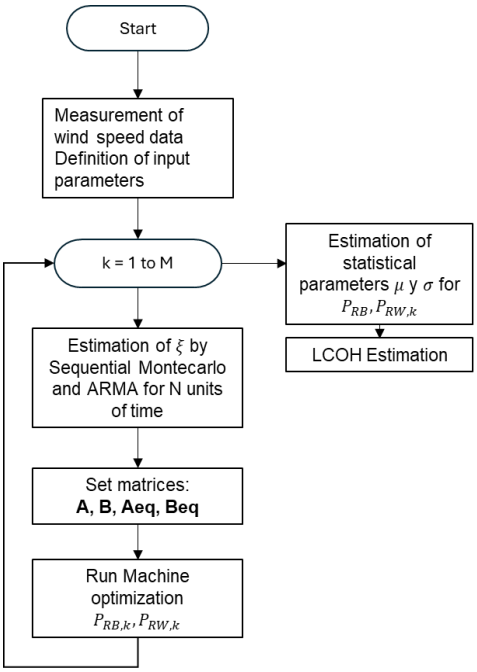

Figure 7. Monte Carlo simulation

4. CASE OF STUDY

This study considers two scenarios, as illustrated in Figure 5. In the first scenario (case 1), a wind power plant and a BESS are used to provide continuous power for hydrogen production. In this configuration, the wind power plant injects energy into the grid, while the BESS supplies or absorbs power depending on its operational mode.

The second scenario (case 2) introduces an isolated thermal generator to supplement renewable energy sources. Both configurations are designed to supply a constant load representative of an industrial application. To validate the proposed methodology, wind speed input data were collected in La Guajira, Colombia, during the years 2016 and 2017. Figure 8 displays the measured wind speed data, while Figure 9 presents its histogram and cumulative probability distribution.

For the simulation, 2000 kW wind turbines were selected. Their technical specifications are provided in Table 2, and the corresponding power-wind speed curve is illustrated in Figure 10. The electrolyzer system includes rectifiers, electrolyzer units, and connection cables. Table 3 summarizes the input and output characteristics of the electrolyzer used in the test system. Additionally, Table 4 presents the cost-related parameters associated with the electrolyzer configuration.

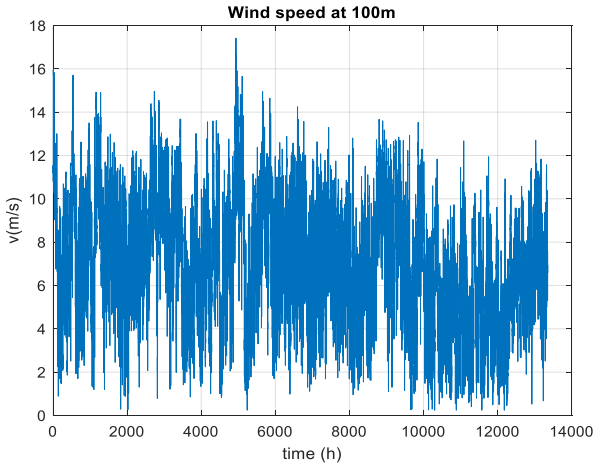

Figure 8. Input data

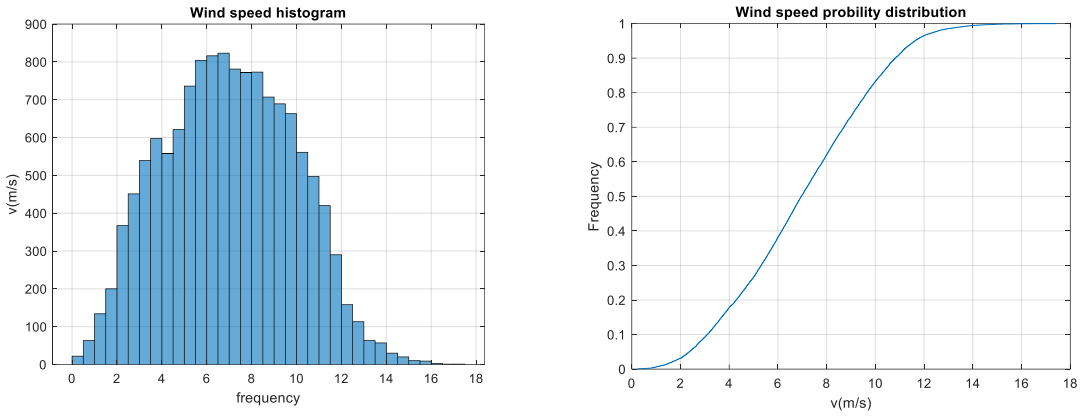

Figure 9. Wind speed histogram and probability distribution

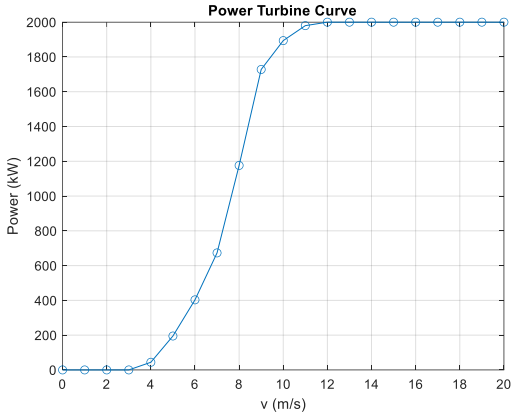

Figure 10. Vestas V110/2000 power curve

Table 2. Turbine data

S.L.	Description	Value	S.L.	Description	Value
1	Brand	Vestas (Daemark)	6	Blades	3
2	Model	V110/2000	7	Wind speed cut on	4 m/s
3	Nominal power	2000 kW	8	Rated wind speed	12 m/s
4	Rotor diameter	110 m	9	Wind speed cut off	20 m/s
5	Class	IEC IIIa	10	Axe height	100 m

Table 3. Electrolyzer data [26]

Inputs		Value
Average power consumption		5000 kW
Water consumption		14.83 L per kg produced hydrogen
Output (hydrogen)	Volume	990 Nm^3/h
	Mass	2125 kg/day (88 kh/h)
	Pression	4 bar/580 psig
Operational	Start time	60 s ramp up
	Average efficiency	49.49 kWh/kg
	Load following	60 s from min. to max. (ramp up) < 15 s from max. to min (ramp down)

Table 4. Cost parameters [4], [12]

Parameter	Value	Parameter	Value
π_w	1200 ($ per installed kW)	b^B_{min}	0.1
π_B	1430 ($ per installed kW)	b^B_{max}	0.9
π_{Th}	0.2 ($ per kw)	τ_B	0.95
e_{DB}	0.995	P_{RE}	5000 kW
e_{CB}	0.975	b^E_{min}	0.8
SDR	0.05	b^E_{max}	1

5. RESULTS

As shown in Figure 7, the ARMA model is constructed using the wind speed data described earlier, following the procedure of section 3.3.3. For this analysis, the econometrics module of MATLAB® is employed. In this case, the autoregressive p and moving average q parameters are set to 3. Table 5 presents the coefficients. Thus, wind speed over the studied period can be estimated using (46).

$$v = u + \sigma x = [v_1 \quad \cdots \quad vt \quad \cdots \quad v_N] \tag{46}$$

Wind speed was predicted over a 20-year period (175,200 hours). A comparison of the probability distributions is presented in Figure 11, showing that the predicted values follow the same distribution as the measured data. The two study scenarios presented in section 4 are simulated using hourly realizations over a 20-year period, assuming 365 days per year. The optimization process is formulated as a MILP problem and is solved in MATLAB using the *intlinprog* function for each realization.

5.1. Case 1

For each analysis, a time window of 24x7x4 hours and 365x20 realizations is considered to run the simulation, which means that the total analysis time is equivalent to 20 years. Figure 12 shows the histogram of the optimization result for BESS and wind power plant sizing. Tables 6 and 7 show the statistical results and the calculation of the LCOH.

Table 5. Statistical parameters ARMA model

Description	Symbol	Value
Autoregressive parameters	θ_1	0.8624
	θ_2	0.8494
	θ_3	-0.7142
Average parameters	ϕ_1	0.2240
	ϕ_2	-0.9009
	ϕ_3	-0.2508
White noise variance	σ_α^2	1.2980

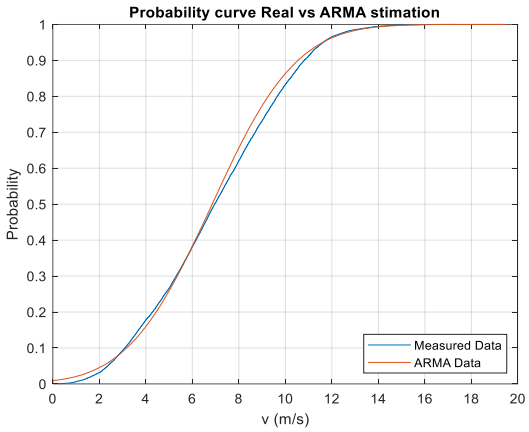

Figure 11. Probability distribution comparison of measured data vs ARMA model

Table 6. Results at 95% confidence interval case 1

Parameter	BESS	Wind power plant
Average (μ)	28.9 MWh	14.8 MWh
Standard deviation (σ)	28.9 MWh	8.8 MW

Table 7. LOCH calculation case 1

Equipment	Value	Unit installed value	Total
BESS	28.9 MWh	1.7 MD per MW-installed	34.6 MD
Wind power plant	14.8 MWh	1.2 MD per MWh-installed	20.7 MD
PEM electrolyzer	5 MW	1.2 MD per MWh-installed	6 MD
		CDF	15417 tn
		LOCH	5.92 $ per H2 kg

5.2. Case 2

Considering the same time window and number of realizations as in case 1, case 2 introduces an isolated thermal power plant, as previously mentioned. Figure 13 presents the histogram of the optimization results obtained from the realizations. Following the same approach as in case 1, Tables 8 and 9 summarize the statistical results and the LCOH calculations.

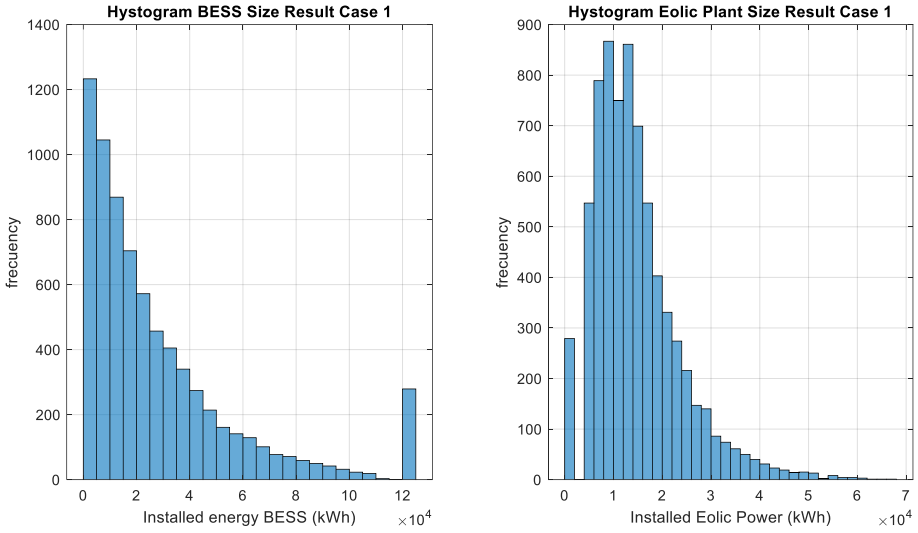

Figure 12. BESS and wind power plant optimal solution histogram for case 1

Table 8. Results at 95% confidence interval case 2

Parameter	BESS	Wind power plant
Average (μ)	28.9 MWh	14.8 MWh
Standard deviation (σ)	28.9 MWh	8.8 MW

Table 9. LOCH calculation case 2

Equipment	Value	Unit installed value	Total
BESS	17.6 MWh	1.7 MD per MW-installed	34.6 MD
Wind power plant	15.2 MWh	1.2 MD per MWh-installed	20.7 MD
PEM electrolyzer	5 MW	1.2 MD per MWh-installed	6 MD
		CDF	15417 tn
		LOCH	3.4 $ per H2 kg

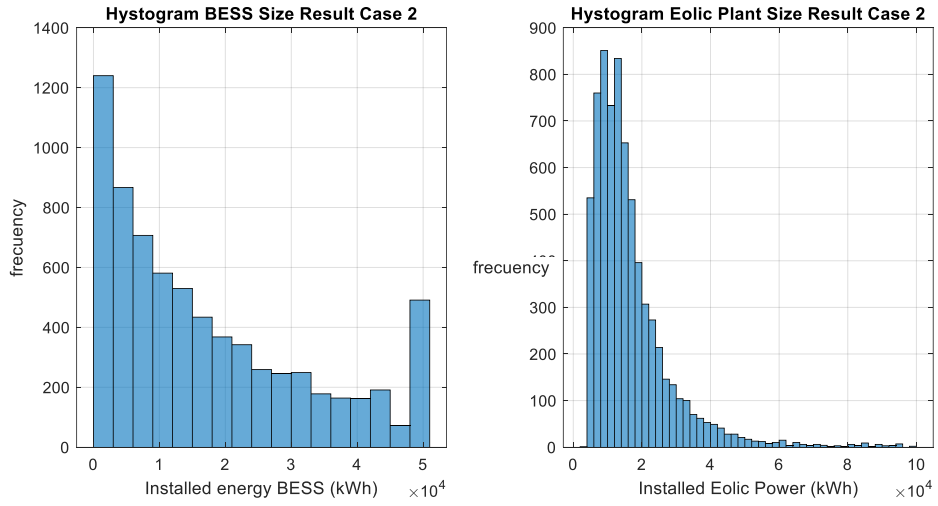

Figure 13. BESS and wind power plant optimal solution histogram for case 2

6. CONCLUSION

This paper presents a comprehensive methodology for sizing the main components - namely, the wind power plant and BESS - in an isolated grid designed to supply a green hydrogen plant, considering the stochastic nature of wind energy. The proposed approach enables the determination of nominal capacities during the feasibility stage of project development. Given that the international LCOH for PEM technology typically ranges between $3 and $6 per kilogram, the results obtained in this study are expected to fall within this benchmark.

The findings suggest that integrating a thermal generator capable of supporting both the base load and, intermittently, the hydrogen plant demand, facilitates daily energy balancing. This is achieved through the application of a sequential Monte Carlo simulation, which introduces a probabilistic dimension to the analysis. As a result, the outcomes inherently include a stochastic component that should be considered in investment decision-making. Moreover, in both scenarios - isolated grid and isolated grid with an auxiliary thermal generator - the required BESS capacities exceed typical nominal values. This indicates that, under certain conditions, the BESS alone may not be sufficient to ensure continuous operation. Therefore, future work should also address the reliability and operational availability of the electrolyzer system. In consequence, future research could expand this methodology by incorporating additional parameters, such as system reliability metrics and the lifecycle characteristics of the BESS.

FUNDING INFORMATION

Authors state no funding involved.

AUTHOR CONTRIBUTIONS STATEMENT

This journal uses the Contributor Roles Taxonomy (CRediT) to recognize individual author contributions, reduce authorship disputes, and facilitate collaboration.

Name of Author	C	M	So	Va	Fo	I	R	D	O	E	Vi	Su	P	Fu
Michael Salcedo	✓	✓	✓	✓	✓	✓	✓	✓	✓	✓			✓	✓
Mario A. Rios		✓			✓	✓		✓	✓	✓	✓	✓	✓	

C : **C**onceptualization
M : **M**ethodology
So : **So**ftware
Va : **Va**lidation
Fo : **Fo**rmal analysis
I : **I**nvestigation
R : **R**esources
D : **D**ata Curation
O : Writing - **O**riginal Draft
E : Writing - Review & **E**diting
Vi : **Vi**sualization
Su : **Su**pervision
P : **P**roject administration
Fu : **Fu**nding acquisition

CONFLICT OF INTEREST STATEMENT

Authors state no conflict of interest.

DATA AVAILABILITY

Data availability is not applicable to this paper as no new data were created or analyzed in this study.

REFERENCES

[1] M. E. Sahin, "An overview of different water electrolyzer types for hydrogen production," *Energies*, vol. 17, no. 19, 2024, doi: 10.3390/en17194944.
[2] J. Wu, X. Qin, H. He, and Z. Yantao, "Peak-shaving requirement analysis method based on sequential monte-carlo simulation for large scale wind power integrated system," in *2018 China International Conference on Electricity Distribution (CICED)*, Sept. 2018, pp. 2007-2012, doi: 10.1109/CICED.2018.8592216.
[3] I. K. Kookos, "Systematic optimization of off-grid green hydrogen production systems," *International Journal of Hydrogen Energy*, vol. 79, no. 19, pp. 1299–1312, doi: 10.1016/j.ijhydene.2024.07.117.
[4] M. G. Dozein, A. M. De Corato, and P. Mancarella, "Virtual inertia response and frequency control ancillary services from hydrogen electrolyzers," *IEEE Transactions On Power Systems*, vol. 38, no. 3, pp. 2447-2459, May 2023, doi: 10.1109/TPWRS.2022.3181853.
[5] S. P. Ntomalis *et al.*, "Optimal siting of BESS in distribution networks under high wind power penetration," *IEEE International Energy Conference (ENERGYCON)*, pp. 1-6, 2018, doi: 10.1109/ENERGYCON.2018.8398771.
[6] T. M. Blasi, T. S. P. Fernandes, A. R. Aoki, and F. H. Tabarro, "Multiperiod optimum power flow for active distribution networks with provisioning of ancillary services," *IEEE Transactions on Energy Conversion*, vol. 11, no. 2, pp. 1-9, June 1996, doi: 10.1109/ACCESS.2021.3101419.

[7] H. Morais, P. Kádár, P. Faria, Z. A. Vale, and H. Khodr, "Optimal scheduling of a renewable micro-grid in an isolated load area using mixed-integer linear programming," *Elsevier Renewable Energy*, vol. 35, pp. 151-156, 2010, doi: 10.1016/j.renene.2009.02.031.
[8] A. Sherature *et al.*, "Assessment of electricity excess in an isolated hybrid energy system: a case study of a Dangiwada village in rural Nepal," *Energy Procedia*, vol. 160, pp.76-83, 2019, doi: 10.1016/j.egypro.2019.02.121.
[9] C. Abbey and G. Joos, "A stochastic optimization approach to rating of energy storage systems in wind-diesel isolated grids," *IEEE Transactions on Power Systems*, vol. 24, no. 1, pp. 418-426, Feb. 2009, doi: 10.1109/TPWRS.2008.2004840.
[10] R. Prajapati and V. K. Garg, "Optimal sizing of standalone small rotor wind and diesel system with energy with energy storage for low speed wind operation," In *2017 4th International Conference on Signal Processing, Computing and Control (ISPCC*), 2017, pp. 440-445, doi: 10.1109/ISPCC.2017.8269719.
[11] J. Pan, A. Chen, Z. Zhao, J. Lei, J. Cao, and Z. Hang, "Optimal proportion of wind, PV, hydrogen and storage capacity based on time sequence simulation," *International Conference on Power and Energy Applications*, 2022, vol. 5th, pp. 657-662, doi: 10.1109/ICPEA56363.2022.10052461.
[12] S. M. Dawoud, X. Lin and M. I. Okba, "Hybrid renewable microgrid optimization techniques: a review," *Elsevier Renewable and Sustainable Energy Reviews*, vol. 82, p. 2039–2052, 2018, doi: 10.1016/j.rser.2017.08.007.
[13] J. Incer-Valverde, A. Korayem, G. Tsatsaronis, and T. Morosuk, "'Colors' of hydrogen: definitions and carbon intensity," *Energy Conversion and Management*, vol. 291, no. 117294, Sept. 2023, doi: 10.1016/j.enconman.2023.117294.
[14] I. Toure, A. Payman, M.B. Camara, and B. Dakyo, "A review on electrolyser and hydrogen production," in *11th International Conference on Smart Grid (icSmartGrid)*, Paris, France, June 2023, doi: 10.1109/icSmartGrid58556.2023.10171040.
[15] S. F. Amireh *et al.*, "Impact of power supply fluctuation and part load operation on the efficiency of alkaline water electrolysis," *Journal of Power Sources*, vol. 560, no. 232629, 2023, doi: 10.1016/j.jpowsour.2023.232629.
[16] Shiva Kumar and V. Himabindu, "Hydrogen production by PEM water electrolysis – a review," *Materials Science for Energy Technologies*, vol. 2, pp. 442–454, 2019, doi: 10.1016/j.mset.2019.03.002.
[17] R. Fernandez, L. Martinez, R. Peña, and R. Mantz, "Electrolyzers as smart loads, preserving the lifetime," *International Journal of Hydrogen Energy*, vol. 52, pp. 72-79, 2024, doi: 10.1016/j.ijhydene.2023.11.174.
[18] K. Koiwa, L. Cui, T. Zanma, K.Z. Liu, and J. Tamura, "A coordinated control method for integrated system of wind farm and hydrogen production: Kinetic energy and virtual discharge controls," *IEEE Access*, vol. 10, pp. 28283-28294, March 2022, doi: 10.1109/ACCESS.2022.3158567.
[19] J. Lei, H. Ma, G. Qin, Z. Guo, P. Xia, and C. Hao, "A comprehensive review on the power supply system of hydrogen production electrolyzers for future integrated energy systems," *Energies*, vol. 17, no. 4, p. 935, 2024, doi: 10.3390/en17040935.
[20] J. Eichman, K. Harrison, and M. Peters, "Novel electrolyzer applications: providing more than just hydrogen," *National Renewable Energy Laboratory*, vol. 5400, no. 61758, pp. 1-35, 2014.
[21] H. Alharbi and K. Bhattacharya, "Stochastic optimal planning of battery energy storage systems for isolated microgrids," *IEEE Transactions on Sustainable Energy*, vol. 9, no. 1, pp. 211-227, 2018, doi: 10.1109/TSTE.2017.2724514.
[22] M. Kumar Kar, S. Kanungo, S. Dash, and R. N. R Parida, "Grid connected solar panel with battery energy storage system," *International Journal of Applied Power Engineering (IJAPE),* vol. 13, no. 1, pp. 223-233, 2024, doi: 10.11591/IJAPE.V13.I1.PP223-233.
[23] G. Pflug and A. Pichler, *Multistage stochastic optimization*, New York: Springer, 2014.
[24] C. Chatfield, *Analysis of time series: an introduction*, Bath, Avon: Chapman & Hall/CRC, 1995.
[25] M. Miller, J. L. Paternina, S. F. Contreras, C. A. Cortes, and J. M. A. Myrzik, "Optimal allocation of renewable energy systems in a weak distribution," *Electric Power Systems Research*, vol. 235, no. 110649, 2024, doi: 10.1016/j.epsr.2024.110649.
[26] Plug Power Inc., "Plug EX-2125D electrolyzer," Apr. 2022. [Online]. Available: https://resources.plugpower.com/electrolyzers/ex-2125d-f041122.

BIOGRAPHIES OF AUTHORS

Michael Salcedo received a degree in electrical engineering in 2015, from National University, Bogota, Colombia. Currently, he is a student of a Master of Science degree in electrical engineering at the University of Los Andes. With experience of engineering electrical applied in petrochemical and energy transition projects, his areas of interest are large scale integration of non-conventional sources of energy, decarbonization projects, and industrial applications. He can be contacted at email: ma.salcedo23@uniandes.edu.co.

Mario A. Rios received a degree in electrical engineering in 1991 and a M.Sc. degree in electrical engineering in 1992, both from Universidad de los Andes, Bogota, Colombia. He received a Ph.D. degree in electrical engineering from INPG-LEG, Grenoble, France, in 1998, and a doctoral degree in engineering from Universidad de los Andes, in 1998. He worked as a consultant engineer in ConCol (now WSP), Bogotá, Colombia, during 12 years. Also, he was a research associate at the University of Manchester (formerly, UMIST). Currently, he is full professor at the Department of Electrical Engineering, School of Engineering, Universidad de los Andes, Bogotá. He can be contacted at email: mrios@uniandes.edu.co.